Journal of Inflammation Research

Dovepress
Taylor & Francis Group

Open Access Full Text Article

ORIGINAL RESEARCH

Huanglian Jiedu Decoction Alleviates Myocardial Ischemia-Reperfusion Injury via AKT-Mediated Regulation of Endoplasmic Reticulum Stress

Mingyang Gu[1–4], Jiongbo Xu[1–4], Zhihan Liao[2,4], Jinhai Lin[2], Rui Li[5], Wei Wu[1,6], Yijun Qiu[1,2]

[1]The First Affiliated Hospital of Guangzhou University of Chinese Medicine, Guangzhou, People's Republic of China; [2]Guangzhou University of Chinese Medicine, Guangzhou, People's Republic of China; [3]The First Clinical Medical College, Guangzhou University of Chinese Medicine, Guangzhou, People's Republic of China; [4]Science and Technology Innovation Center, Guangzhou University of Chinese Medicine, Guangzhou, People's Republic of China; [5]Department of Emergency, The First Affiliated Hospital of Guangzhou University of Chinese Medicine, Guangzhou, People's Republic of China; [6]Guangdong Clinical Research Academy of Chinese Medicine, Guangzhou, People's Republic of China

Correspondence: Wei Wu; Yijun Qiu, Email zywuwei@163.com; yijun.qiu@163.com

Purpose: Modulation of the AKT signaling pathway can effectively regulate endoplasmic reticulum stress (ERS) and inhibit ischemia-induced cardiomyocyte apoptosis in myocardial ischemia-reperfusion injury (MIRI). The present study was designed to investigate the role of AKT and ERS in the modulation of MIRI by Huanglian Jiedu Decoction (HLJDD) through in vitro and in vivo experiments.

Methods: In vivo studies employed a rat model of MIRI with three HLJDD dosage groups and a nicorandil control group. Comprehensive evaluations were conducted, including assessments of cardiac function, histopathological analysis, apoptosis detection, and immunohistochemical examination of ERS markers. For in vitro validation, H9c2 cardiomyocytes were subjected to hypoxia/reoxygenation conditions, and cellular viability assays were combined with ultrastructural and molecular analyses. Investigations guided by network pharmacology focused on the PERK/eIF2α/CHOP signaling pathway and AKT phosphorylation.

Results: HLJDD demonstrated dose-dependent cardioprotective effects through attenuation of myocardial apoptosis and ERS activation. Mechanistic studies revealed its ability to restore AKT phosphorylation and suppress the PERK/eIF2α/CHOP signaling cascade. The cardioprotective effects were abolished upon AKT inhibition, thereby confirming the specificity of this pathway.

Conclusion: HLJDD may serve as a potential therapeutic candidate for ischemia-induced cardiomyocyte apoptosis during MIRI. HLJDD exerts its effects by inhibiting the AKT-mediated PERK/eIF2α/CHOP signaling pathway, attenuating ERS and thereby reducing MIRI-induced apoptosis.

Keywords: myocardial ischemia-reperfusion injury, Huanglian Jiedu Decoction, cardiomyocyte apoptosis, endoplasmic reticulum stress, AKT

Introduction

Ischemic cardiovascular disease is universally recognized as the leading global cause of mortality, with its pathogenesis closely associated with hemodynamic abnormalities.[1,2] Current clinical strategies primarily focus on revascularization through interventional techniques (angioplasty/percutaneous coronary intervention) combined with pharmacological interventions (anticoagulants, antiplatelet agents, nitroglycerin, and thrombolytics)[3] to optimize coronary perfusion. Nevertheless, reperfusion may paradoxically induce myocardial ischemia/reperfusion injury (MIRI), a pathophysiological condition strongly correlated with severe complications, including myocardial stunning, malignant arrhythmias, and heart failure.[4]

Accumulating evidence identifies cardiomyocyte apoptosis and endoplasmic reticulum stress (ERS) as decisive checkpoints in ischemia/reperfusion (I/R) injury,[5] and pharmacologic suppression of ERS has consistently conferred cardioprotection in preclinical models.

Received: 4 June 2025
Accepted: 18 November 2025
Published: 3 December 2025

Graphical Abstract

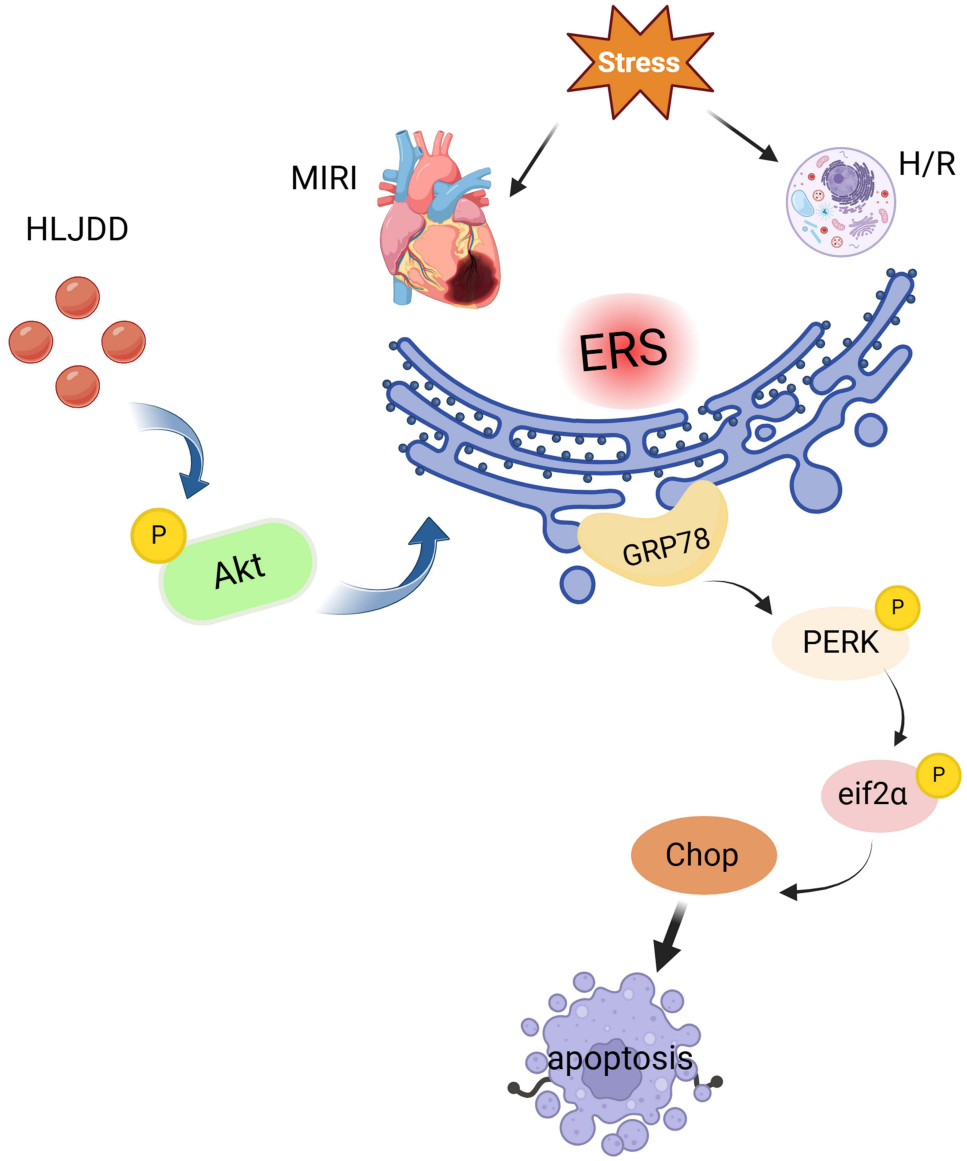

Mechanistically, I/R impairs ATP synthesis, triggers oxidative stress, and disrupts Ca^{2}+ homeostasis. The resulting accumulation of misfolded proteins in the endoplasmic reticulum (ER) lumen triggers the unfolded-protein response (UPR), characterized by elevated glucose-regulated protein 78 (GRP78) and synchronized activation of three canonical sensors: inositol-requiring enzyme 1α (IRE1α), protein kinase R-like ER kinase (PERK), and activating transcription factor 6 (ATF6).[6–8]Hyperactivation of the PERK–eIF2α–CHOP (C/EBP homologous protein) axis, in particular, propagates ERS-driven apoptotic cascades.

The PI3K/AKT arm of the reperfusion-injury salvage kinase (RISK) pathway simultaneously governs cell survival and ERS-related apoptosis.[9–11] A robust, inverse correlation between phospho-AKT (p-AKT, Ser473) abundance and ERS-mediated apoptosis has further established AKT as a critical rheostat that restrains reperfusion-induced cellular stress.[12]

Traditional Chinese medicine (TCM) is a multi-component, synergistic therapeutic system refined over millennia of clinical practice in East Asia. By targeting multiple molecular sites and regulating systemic metabolic networks, TCM

formulae offer a mechanistically distinct strategy for complex, multifactorial diseases. Consequently, botanical preparations with cardioprotective activity have become a focal point of contemporary pharmacological investigation. Huanglian Jiedu Decoction (HLJDD), a classical heat-clearing formula composed of Coptis chinensis Franch. (Huanglian, Coptidis Rhizoma; 30 g), Scutellaria baicalensis Georgi (Huangqin, Scutellariae Radix; 20 g), Phellodendron chinense C.K. Schneid. (Huangbo, Phellodendri Chinensis Cortex; 20 g), and Gardenia jasminoides J. Ellis (Zhizi, Gardeniae Fructus; 30 g), has been scientifically confirmed to contain pharmacologically active constituents, including alkaloids, flavonoids, and iridoid glycosides.[13] Modern pharmacological studies verify that this formula exhibits broad-spectrum anti-inflammatory, antibacterial, antioxidant, metabolic regulatory, and neuroprotective properties.[14] In cardiovascular therapeutics, clinical practice demonstrates its frequent application as an adjuvant treatment. Emerging research indicates that HLJDD effectively attenuates metabolic disorder-induced myocardial injury through targeted modulation of inflammation-mediated insulin resistance. Our preliminary studies show it plays a key role in preventing atherosclerosis and regulating lipid metabolism homeostasis via modulating the P2RY12/PI3K/AKT signaling pathway.[15] Pharmacodynamic investigations further demonstrate that Scutellaria baicalensis extract enhances catalase activity and improves vascular elasticity, thereby reducing myocardial ischemia-reperfusion injury.[16] At the same time, characteristic alkaloids in HLJDD (eg, berberine and palmatine) significantly mitigate acute myocardial tissue damage induced by ischemia-reperfusion through inhibition of cardiomyocyte autophagy activation, regulation of oxidative stress balance, and modulation of inflammatory cytokine networks.[17,18]

Although existing studies have preliminarily elucidated the cardioprotective effects of HLJDD, key scientific issues, such as its multi-component synergistic mechanisms, pharmacodynamic material basis, and signaling pathway network regulation, still require systematic and in-depth investigation. Network pharmacology, as an emerging discipline integrating systems biology and polypharmacology, provides methodological support for elucidating the "multi-component, multi-target, multi-pathway" action mode of TCM formulas. This technology effectively predicts active ingredient clusters and their synergistic mechanisms through constructing compound-target-disease interaction networks, which aligns well with the holistic perspective of TCM.

Based on this background, the present study aims to investigate: 1) The protective effects of HLJDD against I/R injury; 2) Whether AKT signaling-mediated regulation of ERS contributes to its cardioprotective mechanisms. The findings will provide theoretical evidence for clarifying the multi-target action characteristics of HLJDD.

Materials and Methods

Animals

A total of 48 male Sprague-Dawley (SD) rats (8–10 weeks old) with initial body weights of 180 ± 20g specific pathogen −free (SPF) grade were obtained from the Laboratory Animal Center of Southern Medical University (Animal Production License No: SCXK[Yue]2021–0041). The animals were housed in the SPF-grade barrier facility at the Experimental Animal Center of The First Affiliated Hospital of Guangzhou University of Chinese Medicine (Animal Use License No: SYXK[Yue]2023–0092). All experimental procedures strictly adhered to the internationally recognized 3R principles —— Replacement, Reduction, and Refinement and were approved by the Institutional Animal Care and Use Committee of The First Affiliated Hospital of Guangzhou University of Chinese Medicine (Ethical Approval No.: GZTCMF1-20230054).

Main Reagents

The Chinese herbal medicines of HLJDD were provided by the Pharmacy Department of the First Affiliated Hospital of Guangzhou University of Chinese Medicine (Coptischinensis, 30g, Scutellariabaicalensis, 20g, Phellodendronchinense, 20g, and Gardeniajasminoides, 30g. The preparation process was as follows: Herbs were soaked in water for 1 hour, decocted twice, filtered through filter paper twice, and aliquoted. The solution was centrifuged at 11,000×g for 15 min at 4°C to collect supernatant. The supernatant was concentrated to 100 mL using a rotary evaporator at 60°C, followed by lyophilization in a vacuum freeze-dryer. Details of the lyophilized powder can be found in the team's previous research[15]); Nicorandil (N129566,Shanghai Aladdin, China); GRP78 Antibody (11587−1−AP,Proteintech); Bcl-2

Antibody (AF6139,Affinity); Bax Antibody (AF0120,Affinity); Caspase-3 Antibody (AF6311, Affinity); PERK Antibody (AF5304,Affinity); Phospho-PERK Antibody (DF7576, Affinity); eIF2α Antibody (AF6087,Affinity); Phospho-eIF2α Antibody (AF3087, Affinity); CHOP Antibody (15204−1−AP,Proteintech); AKT Antibody (AF6261, Affinity); Phospho-AKT Antibody (66,444−1−1g,Proteintech); β-actin Antibody (21338,SAB); Goat anti-rabbit IgG (SA00001−2,Proteintech); HRP-labeled goat anti-rabbit IgG (5220−0336,SeraCare); Creatine Kinase-MB (CK−MB) Assay Kit (H197−1−1,Nanjing Jiancheng,China); Lactate Dehydrogenase (LDH) Kit (A020−2−2,Nanjing Jiancheng, China); MK-2206 (HY−10358,MCE,USA).

MI/R Model Establishment and Animal Grouping

Following anesthesia with 0.3% sodium pentobarbital via intraperitoneal injection, experimental animals were maintained at 37°C using a thermostatic heating pad. After tracheal intubation, mechanical ventilation was initiated using a rodent respirator with parameters set at an inspiration-expiration ratio of 1:1, tidal volume of 6–10 mL/kg, and respiratory rate of 70 ± 10 breaths/min. Myocardial ischemia-reperfusion injury was induced through left lateral thoracotomy with polyethylene catheter-protected ligation of the left anterior descending coronary artery for 30 minutes, followed by 120 minutes of reperfusion.[19,20] After the MIRI model was successfully established, blood and left ventricular tissue samples were subsequently collected from the rats for subsequent experiments.

The successful establishment of MIRI model was confirmed by three criteria: ①Significant weakening of myocardial contractility distal to the ligation site; ②Ischemic myocardium transitioning from bright red to pale coloration; ③Real-time ECG monitoring demonstrating ST-segment elevation ≥0.2 mV with upward convexity.

Forty-eight SD rats were randomly allocated into six experimental groups (n=8): ①Sham group: thoracotomy without ligation+ normal saline; ②MIRI group: thoracotomy with ligation+ normal saline; ③Low-dose HLJDD group: MIRI + 2.7g/kg; ④Medium-dose HLJDD group: MIRI+ 5.4g/kg; ⑤High-dose HLJDD group: MIRI+ 10.8g/kg; ⑥Positive control group: MIRI+ Nicorandil 6.3mg/kg. The in vivo doses of HLJDD were extrapolated from human clinical doses to animal equivalent doses via body surface area conversion, with the low dose corresponding to the human equivalent dose. HLJDD was administered to animals two weeks before MIRI model establishment.

Electrocardiogram Monitoring in Rats

The rats were anesthetized and fixed supine on the operating table Then, according to the lead pattern (red for the right upper limb, yellow for the left upper limb, green for the left lower limb, and black for the right lower limb), electrode needles were inserted subcutaneously into the rat limbs. Subsequently, the electrodes were connected to the lead wires and then to the electrocardiograph machine to record the electrocardiogram waveforms.

Detection of LDH and CK-MB Levels

Serum samples and cell culture supernatants were collected. The concentrations of Creatine Kinase-MB (CK−MB) and Lactate Dehydrogenase (LDH) were quantitatively measured using commercial enzyme-linked immunosorbent assay ELISA kits in strict accordance with the manufacturer's protocols.

Hematoxylin–Eosin Staining of Myocardial Tissue

Myocardial tissues were fixed in 4% paraformaldehyde solution at room temperature for over 24 hours, followed by paraffin embedding and sectioning into 5-μm-thick slices.[21] Hematoxylin and eosin (HE) staining was performed on myocardial tissue sections for histopathological observation. The stained sections were subsequently subjected to microscopic image acquisition and analysis using the Jiangfeng Digital Pathology Scanning System (Model:KF-FL -005). A double-blind method was adopted for the pathological image analysis of myocardial tissue sections—two pathologists who were not involved in the experimental design independently conducted the scoring, and the average value of their scores was used as the final result to avoid subjective bias.

TUNEL Staining

TUNEL staining was performed using the One-Step TUNEL Apoptosis Detection Kit (Beyotime, C1086) strictly following the manufacturer's protocol. Briefly, paraffin-embedded samples were processed through deparaffinization and rehydration. Antigen retrieval was performed using proteinase K for 25 min, followed by application of TUNEL reaction mixture and incubation at 37°C for 1 h in a light-proof humidified chamber. Finally, sections were mounted with DAPI-containing antifade mounting medium. Fluorescent images were captured and analyzed using the Jiangfeng Digital Pathology Scanning System (Model:KF-FL-005).

Detection of GRP78 with Immunohistochemistry

Paraffin-embedded sections were subjected to microwave-based antigen retrieval using EDTA buffer. Non-specific binding was blocked with 5% bovine serum albumin (BSA) in phosphate-buffered saline (PBS) at room temperature for 30 minutes. The sections were then incubated with a primary antibody against GRP78 diluted 1:200 at 4°C overnight. On the following day, the slides were washed and incubated with a horseradish peroxidase HRP-conjugated secondary antibody at 37°C for 30 minutes. Color development was performed using 3,3′-diaminobenzidine (DAB) as the chromogen, followed by nuclear counterstaining with hematoxylin. Finally, the sections were dehydrated, mounted with neutral resin, and visualized under the Jiangfeng Digital Pathology Scanning System (Model: KF−FL−005) for image acquisition and analysis.

Western Blot

Following protein extraction from cardiac tissues or processed cellular specimens via lysis buffer, protein concentrations were quantitatively determined using the bicinchoninic acid (BCA) assay. Samples were mixed with loading buffer at appropriate ratios and subjected to denaturation in a boiling water bath. Protein separation was achieved through sodium dodecyl sulfate-polyacrylamide gel electrophoresis (SDS-PAGE) following standard Western blot protocols. Post-electrophoretic transfer onto polyvinylidene fluoride (PVDF) membranes was performed, followed by a 2-hour blocking step with 5% skim milk. Primary antibody incubation was conducted overnight at 4°C, with subsequent TBST buffer washes to remove unbound antibodies. Secondary antibody incubation proceeded for 1 hour at room temperature. Chemiluminescent detection was implemented using an ECL kit according to manufacturer specifications, with PVDF membranes visualized through a Bio-Rad gel imaging system. Quantitative analysis of band intensity was ultimately performed using Image J software.

Cell Line

The H9c2 cell line was procured from Procell Life Science & Technology Co., Ltd., Wuhan, China and cultured in DMEM medium (Servicebio, G4612) supplemented with 10% fetal bovine serum (FBS, Sigma, F7524), 100 mg/mL streptomycin and 100 IU/mL penicillin (Biosharp, BL505A). Cells were maintained under standard culture conditions at 37°C in a humidified incubator with 5% CO_2 and 95% air atmosphere.

Establishment of H/R Model and Grouping

An in vitro ischemia-reperfusion model was simulated by using hypoxia-reoxygenation. The conditions were hypoxia (5% CO_2 and 95% N_2) for 8 hours, followed by reoxygenation (5% CO_2 and 95% O_2) for 3 hours. The cells were randomly divided into 6 groups: (1) Control group: Normal H9c2 cells under normoxic conditions; (2) H/R group: The model group with 8 hours of hypoxia and 3 hours of reoxygenation; (3) H/R + HLJDD group: HLJDD (160 μg/mL) was dissolved in cell culture medium and used to pre-treat cells for 24 hours before reoxygenation; (4) H/R + MK-2206 group: 5.0 μM MK-2206 was pre-treated for 24 hours before hypoxia; (5) H/R + MK-2206 + HLJDD group: 160 μg/mL HLJDD and 5.0 μM MK-2206 were pre-treated for 24 hours before hypoxia. For the control group and the H/R group, an equal volume of 100% DMSO (instead of the drug stock solution) was diluted in the cell culture medium to achieve a final DMSO concentration of 0.1% (v/v), which was identical to that in the MK-2206-treated groups. Passages 5–10 of the H9c2 cell line were used for the experiments. Each experiment was repeated at least three times.

Cell Viability

According to the manufacturer's instructions, the cell viability of H9c2 cells was analyzed by the Cell Counting Kit-8 (CCK-8) method. Briefly, H9c2 cells in the logarithmic growth phase were seeded into 96-well plates and cultured overnight at 37 °C with 5% CO_2. After a series of interventions, 10 μL of CCK-8 solution (Biosharp, BS350A) was added to each well. After incubation at 37 °C for 2 hours, the optical density (OD) at 450 nm was measured using a microplate reader. The viability was calculated according to the formula: Viability (%) = (OD of experimental group-OD of blank control group)/ (OD of normal control group-OD of blank control group) × 100%.

LDH Activity

The reaction system was prepared according to the manufacturer's instructions. Following the addition of 2,4-dinitrophenylhydrazine, the mixture was incubated at 37 °C for 15 min in a thermostatic incubator. Subsequently, 0.4 mol/L NaOH solution was added to terminate the reaction, followed by a 5 min incubation at room temperature. Finally, LDH content in each well was quantitatively determined using a microplate reader at a measurement wavelength of 450 nm.

Apoptosis Assay

The cell samples were fixed with 4% paraformaldehyde for 30 min and permeabilized with 0.3% Triton X-100 solution for 10 min. Subsequently, the prepared TUNEL reaction mixture was added and incubated at 37°C for 1 hour protected from light. Finally, the samples were mounted with an anti-fade mounting medium containing DAPI and observed under an inverted fluorescence microscope (Leica, DMi8, Germany).

Transmission Electron Microscopy

The cells were fixed in 1% osmium tetroxide for 2 hours, followed by gradient dehydration of the samples using ethanol. The specimens were subsequently embedded and polymerized at 60°C for 48 h. Ultrathin sections 60 nm were precisely prepared from the cured samples using an ultramicrotome, then stained with 2% uranyl acetate-lead citrate.[22] Ultrastructural observations were conducted under 5000× and 10,000× magnification using a transmission electron microscope (JEO, L1400, Japan).

Immunofluorescence

H9c2 cardiomyocytes cultured in 24-well plates were fixed with 4% paraformaldehyde at room temperature for 20 min. After microwave-mediated antigen retrieval and membrane permeabilization, samples were blocked with 10% goat serum for 30 min at room temperature. Primary antibodies against GRP78 and CHOP were applied for overnight incubation at 4°C. Following PBS washing the next day, species-matched secondary antibodies were incubated at 37°C for 1 h, followed by tyramide-488/Cy3 application to cell monolayers with 20 min room temperature incubation. Finally, coverslips were mounted on glass slides using DAPI-containing anti-fade mounting medium. Fluorescent images were acquired using a panoramic fluorescence microscope (3DHISTECH Pannoramic MIDI). Fluorescence intensity was quantified using ImageJ software.

Quantitative Real-Time PCR Analysis

Total RNA was isolated from cultured H9c2 cardiomy cells using TRIzol reagent (Thermo Fisher Scientific,15596026CN), cDNA synthesis was performed with PrimeScript™ RT Master Mix (TakaraBio, RR036A) following the manufacturer's protocol. Quantitative real-time PCR analysis was conducted using TB Green® Premix Ex Taq™ II (TakaraBio, RR820A) on a Real-Time PCR System (Bio-Rad, CFX Connect). The comparative Ct method was employed for mRNA quantification, with β-actin serving as the endogenous control. All reactions were performed in triplicate, and mRNA levels were calculated using the $2^{-\Delta\Delta Ct}$ method.

The PCR primer sequences are as follows:

PERK forward: 5'- TTGAAGACTCTGGCTGTGATAATGC −3'

PERK reverse: 5'- CTGCTGCTGGAGTGCTTGAAC −3'
eIF2α forward: 5'- GTCCTCGCAACGCAGCATTC −3'
eIF2α reverse: 5'- AACATCCCATACTTCCATTTGTCCTC −3'
CHOP forward: 5'- AAGGAGAAGGAGCAGGAGAATGAG −3'
CHOP reverse: 5'- GAGCCCGCCGTGTGGTC −3'
GRP78 forward: 5'- GGAGGAGGACAAGAAGGAGGATG −3'
GRP78 reverse: 5'- TTGAATACACCGACGCAGGAATAG −3'
β-actin forward: 5'- ACTGCCGCATCCTCTTCCTC −3'
β-actin reverse: 5'- GAACCGCTCATTGCCGATAGTG −3'

Network Pharmacological Analysis

Identification of HLJDD and MIRI Targets

The screening of active pharmaceutical ingredients was conducted using the TCMSP database (http://tcmspw.com/tcmsp.php, Accessed on March 1st, 2024). With "Scutellaria baicalensis", "Coptis chinensis", "Phellodendron amurense", and "Gardenia jasminoides" as the search keywords, the screening thresholds were set as oral bioavailability (OB) ≥ 30% and drug-likeness (DL) ≥ 0.18. Target prediction was carried out on the Swiss Target Prediction platform. After importing the SMILES structural formulas of each ingredient into the system, the targets were ranked in descending order of prediction probability. Low-confidence targets (prediction probability = 0) were removed, and target genes with a prediction probability higher than the platform's average were retained as candidate targets. Disease-related targets were obtained through joint retrieval in multiple databases. Using "Myocardial ischemia reperfusion injury" and "Ischemia-reperfusion injury" as search terms, target information was retrieved from the GeneCards, OMIM, PharmGkb, and DisGeNET databases[23–25] respectively. Redundant data were removed through integrated analysis. All target information was standardized for gene names via the Uniprot database (http://www.uniprot.org/, Accessed on March 1st, 2024).

Screening of Common Targets of Drugs and Diseases

A Venn diagram of the intersecting genes was created using Venny 2.1 https://bioinfogp.cnb.csic.es/tools/venny/, Accessed on March 1st, 2024). On the homepage of the online tool, the targets corresponding to the active ingredients and the targets related to myocardial ischemia-reperfusion injury (MIRI) were imported. After adjusting the parameters, the Venn diagram was exported to explore the targets of Huanglian Jiedu Decoction in treating MIRI.

Construction and Topological Analysis of the Core Network

The software Cytoscape was used to construct the network diagram. Working files (network file and Type file) were created based on the active ingredients obtained through the above-mentioned methods, their corresponding action targets, and MIRI-related genes. These files were imported into the Cytoscape software. After appropriately adjusting the relevant parameters, the network target diagram was exported. Meanwhile, the "Network Analyzer" tool was used to screen the active targets. The active targets were obtained by arranging them in descending order according to the "Degree" value.

Construction of the Protein-Protein Interaction Network

A protein-protein interaction network was constructed based on the STRING database (http://string-db.org, Accessed on March 1st, 2024), with the confidence threshold set at > 0.7. The set of common targets obtained through screening was imported into the analysis platform. After obtaining the standardized interaction data, network visualization reconstruction was carried out using the Cytoscape software. Further, the Cytohub plugin was used for two rounds of topological screening based on the maximum neighborhood component algorithm (MMC), and finally 8 key core target genes were determined.

Enrichment Analysis of the Intersection Genes

Multidimensional functional annotation was carried out using the DAVID Bioinformatics Resources (https://david.ncifcrf.gov/, Accessed on March 1st, 2024). The screening condition was set as $P < 0.05$. The Gene Ontology (GO)

analysis included three parts: biological process (BP), cellular component (CC), and molecular function (MF). The most relevant signaling pathways were obtained through the Kyoto Encyclopedia of Genes and Genomes (KEGG) analysis, and bubble charts and bar charts were drawn.

Statistics

Data are presented as mean ± standard deviation. All statistical analyses were conducted with GraphPad Prism version 10.1.2 (GraphPad Software, Inc., San Diego, CA, USA). When the sample data did not conform to a normal distribution, nonparametric tests were used. When the data conformed to a normal distribution, a one-way ANOVA was used, and groups were compared using the Dunnett's or Turkey's method. P-value < 0.05 was considered statistically significant. All experiments were repeated at least three times.

Results

HLJDD Attenuated Serum Biomarkers and Cardiac Histopathological Injury

As shown in Figure 1A, significant ST-segment elevation was observed in rats' electrocardiograms during ischemia, with gradual recovery during reperfusion, confirming successful establishment of the MIRI model. Compared with the sham group, the model group exhibited significantly increased LDH levels (7009 ± 544.4 vs 875.6 ± 137.2, P<0.001) (Figure 1B) and CK-MB activity (2673 ± 543.1 vs 582.8 ± 104.1, P<0.001) (Figure 1C). The HLJDD treatment groups (L, M, H) and the nicorandil group effectively attenuated these elevations (all P<0.05), with analogous results observed between the H group and the nicorandil group.

HE staining (Figure 1D) revealed intact myocardial architecture with regular fiber arrangement in sham group. The MIRI group showed structural disorganization, cellular swelling, myofibril fragmentation, interstitial edema, and inflammatory infiltration. The HLJDD-treated groups demonstrated dose-dependent improvements: the L group exhibited partial myocardial disarray and leukocyte infiltration, while pathological alterations progressively ameliorated in the M and H groups. Notably, the H group displayed comparable myocardial preservation to nicorandil group.

HLJDD Mitigates Myocardial Apoptosis to Protect Against MIRI

As depicted in Figure 1E–G, TUNEL staining demonstrated that MIRI induced apoptosis in cardiomyocytes. The proportion of TUNEL-positive cells increased to 22.29 ± 2.81% compared to the control group (P < 0.001). Conversely, when compared with the MIRI group, the number of apoptotic cells decreased by approximately 4.9% in the L group (P < 0.05), 5.7% in the M group (P < 0.05), 6.7% in the H group (P < 0.01), and 7.4% in the nicorandil group (P < 0.01).

At the protein level, as presented in Figure 2A–C, I/R caused an elevation in the Bax/Bcl-2 ratio (5.35 ± 0.79 vs 1.00 ± 0.19, P < 0.001) and an increase in the expression of cleaved-caspase 3 (2.18 ± 0.09 vs 1.00 ± 0.21, P < 0.001), suggesting enhanced apoptosis. After treatment with HLJDD and nicorandil, the Bax/Bcl-2 ratio and cleaved-caspase 3 were reduced to different extents. Particularly, the high-dose group of HLJDD and the positive-control nicorandil group exhibited similar effects.

Prediction of the Regulatory Effect of HLJDD on MIRI

PPI, GO, and KEGG analyses of HLJDD against MIRI

Based on data mining techniques, 139 overlapping genes were identified between the 226 therapeutic targets of HLJDD and 1899 disease targets of MIRI (Figure 3A and B). The top eight key targets included JUN, AKT1, MAPK1, ESR1, TP53, IL6, TNF, and IL1β (Figure 3C–E). Venn diagrams and visualizations were constructed accordingly. Enrichment analyses of biological processes (BP), molecular functions (MF), cellular components (CC), and KEGG pathways were performed using the DAVID database.

The results (Figure 3F and G) revealed that BP terms were primarily associated with response to xenobiotic stimulus, positive regulation of gene expression, response to hypoxia, positive regulation of transcription, DNA-templated, negative regulation of apoptotic process, apoptotic processes, response to lipopolysaccharide, positive regulation of

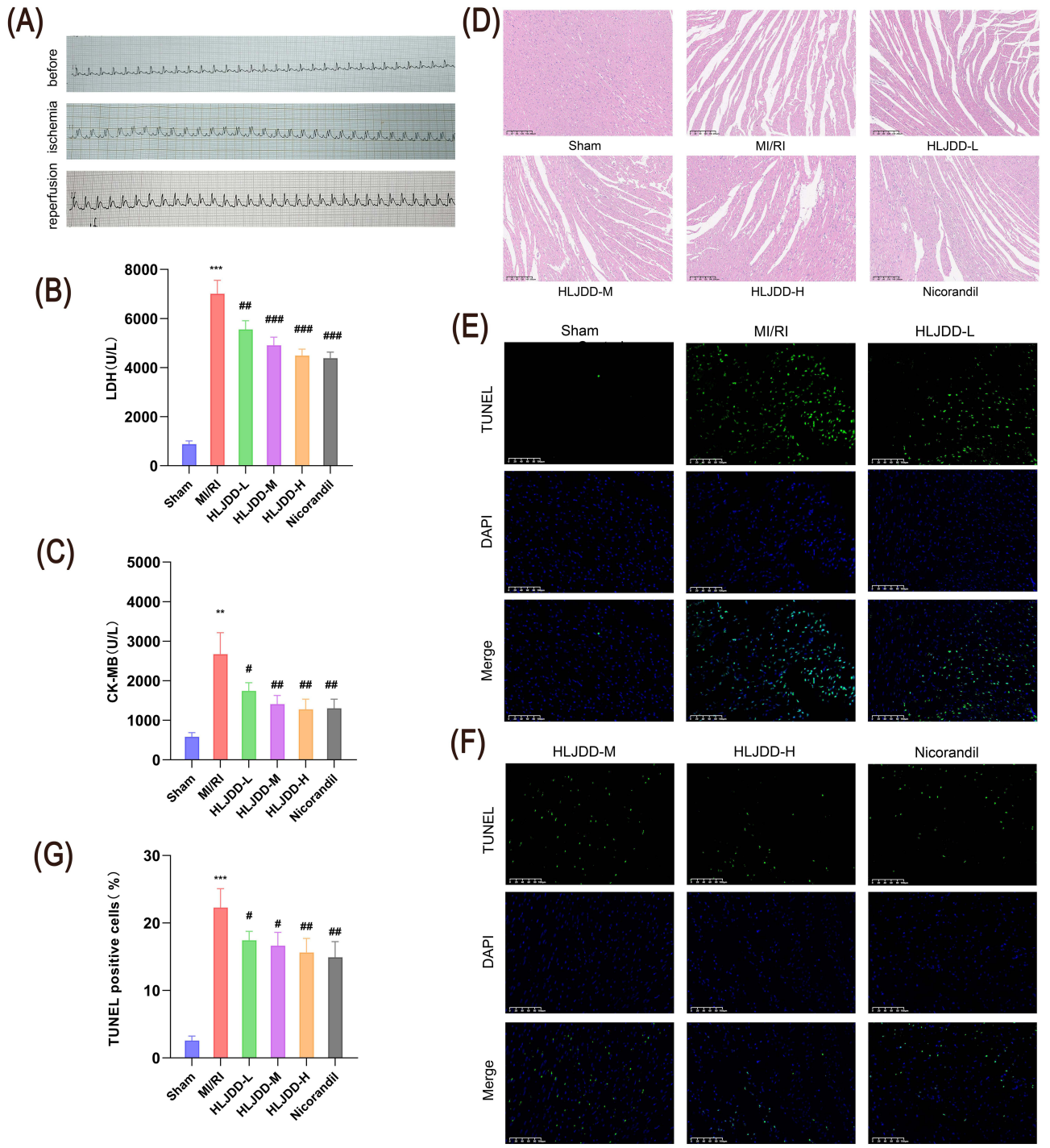

Figure 1 Protective Effects of HLJDD on MIRI Rats. (**A**). Representative ECG images confirming successful MIRI model (lead II). (**B** and **C**). Serum LDH and CK-MB levels in MIRI rats (scale bar: 200 μm; n=6). (**D**). Representative HE-stained cardiac tissue images (n=3). (**E**–**G**). TUNEL assay images and quantitative analysis of cardiac tissue in I/R rats (scale bar: 100 μm; TUNEL: green; DAPI: blue; n=3).

Notes: Data expressed as mean ± SD. **P<0.01, ***P<0.001 vs Sham group; #P<0.05, ##P<0.01, ###P<0.001 vs MI/RI group; ns: no significance.

transcription from RNA polymerase II promoter, positive regulation of apoptotic process and inflammatory response (see Supplementary Table 1). CC terms (Figure 3F and G) were enriched in the extracellular space, membrane raft, extracellular region, caveola, macromolecular complex, cell surface, mitochondria, plasma membrane, perinuclear region of cytoplasm and cytosol (with the endoplasmic reticulum lumen ranked 24th; see Supplementary Table 2). MF terms (Figure 3F and G) included enzyme binding, identical protein binding, protein binding, protease binding, ubiquitin

https://doi.org/10.2147/JIR.S535348

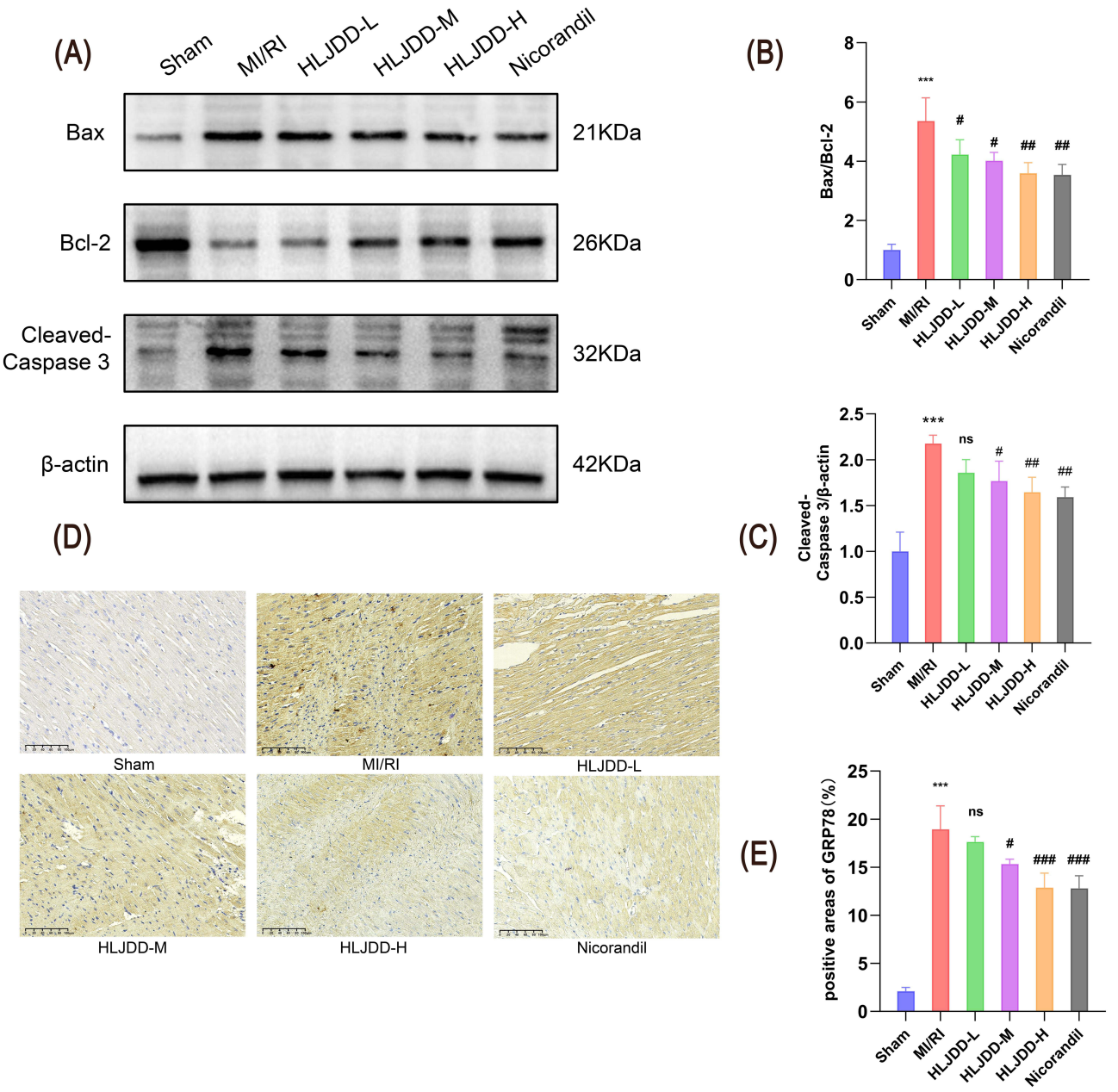

Figure 2 HLJDD Downregulates the Expression of GRP78 and Apoptosis-Related Proteins in MIRI Rats. (**A**–**C**). Western blotting and quantitative analysis of Bax, Bcl-2, and cleaved-caspase 3 in cardiac tissue (n=3). (**D** and **E**). Immunohistochemical analysis of GRP78 expression in cardiac tissue (scale bar: 100 μm, n=3).
Notes: Data expressed as mean ± SD. ***P<0.001 vs Sham group; #P<0.05, ##P<0.01, ###P<0.001 vs MIRI group; ns: no significance.

protein ligase binding, protein homodimerization activity, protein kinase binding, transcription factor activity, sequence-specific DNA binding, RNA polymerase II transcription factor activity, ligand-activated sequence-specific DNA binding and cytokine activity (see Supplementary Table 3). KEGG pathway analysis (Figure 3H and I) highlighted enrichment in Pathways in cancer, Lipid and atherosclerosis, AGE-RAGE signaling pathway in diabetic complications, Fluid shear stress and atherosclerosis, Human cytomegalovirus infection, Hepatitis B, Kaposi sarcoma-associated herpesvirus infection, Hepatitis C, TNF signaling pathway and IL-17 signaling pathway (with PI3K-AKT signaling pathway and Apoptosis ranked 21st and 22nd respectively; see Supplementary Table 4). The top ten GO terms and KEGG pathways were visualized using an online platform based on *P*-values.

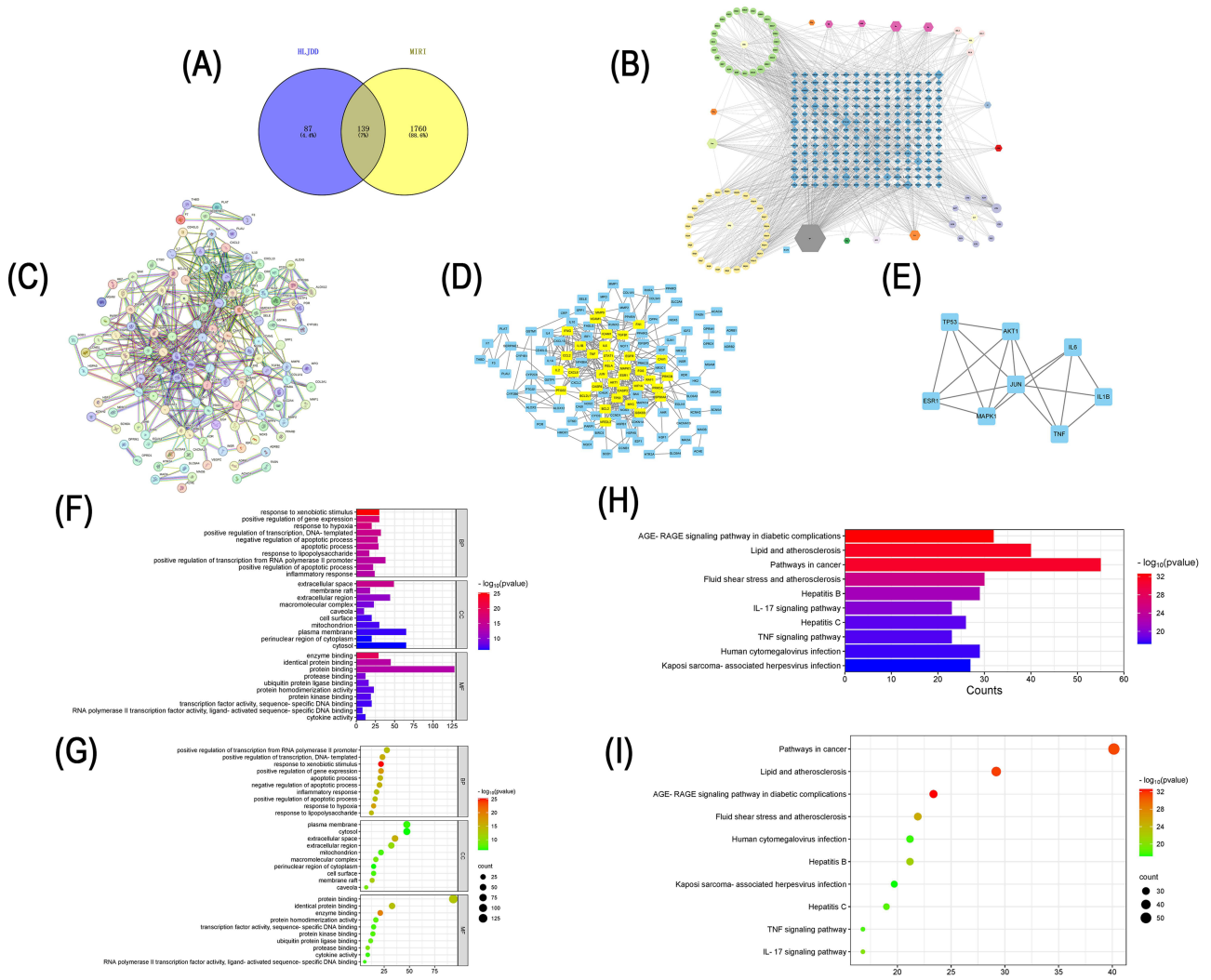

Figure 3 Network Pharmacology Analysis of HLJDD Mechanisms in MIRI. (**A**). Disease-drug target Venn diagram. (**B**). HLJDD compound-target network (**C**–**E**). Screening of core targets. (**F** and **G**). GO analysis. (**H** and **I**). KEGG enrichment analysis.

These findings suggest that the core targets of HLJDD in MIRI treatment are predominantly involved in apoptosis, with multiple processes linked to endoplasmic reticulum activity. GO analysis indicates that HLJDD's therapeutic mechanism against MIRI is closely associated with ERS-induced apoptosis. KEGG enrichment of cancer-related pathways, atherosclerosis, PI3K/AKT signaling, and apoptosis further supports this conclusion, as ERS is a known contributor to cancer, atherosclerosis, and apoptosis regulation.

Immunohistochemical Detection of GRP78 in Vitro

Immunohistochemical results (Figure 2D and E) demonstrated that compared to the control group, the model group exhibited a 9-fold increase in brownish deposits ($P < 0.001$). Both medium- and high-dose HLJDD groups and the nicorandil group showed reduced positive signal intensity compared to the model group ($P < 0.05$, $P < 0.001$, and $P < 0.001$). The high-dose HLJDD group displayed the most significant reduction in deposits (decreased by approximately 6.1%), with the nicorandil group showing a similar effect. Although the low-dose HLJDD group showed a decrease compared with the model group, it was not statistically significant ($P > 0.05$).

https://doi.org/10.2147/JIR.S535348

Validation of AKT-Mediated Endoplasmic Reticulum Stress Mechanisms in the H/R Model

HLJDD Protects H9c2 Cells From H/R-Induced Injury Through AKT Modulation

As illustrated in Figure 4A, HLJDD at concentrations ranging from 20 to 320 μg/mL exhibited no significant impact on H9C2 cell proliferation. Based on other literature and the previous studies of our research group,[19,26] reoxygenation duration was standardized to 3 hours. Subsequent optimization of hypoxia duration demonstrated that subjecting cells to 8-hour hypoxia,

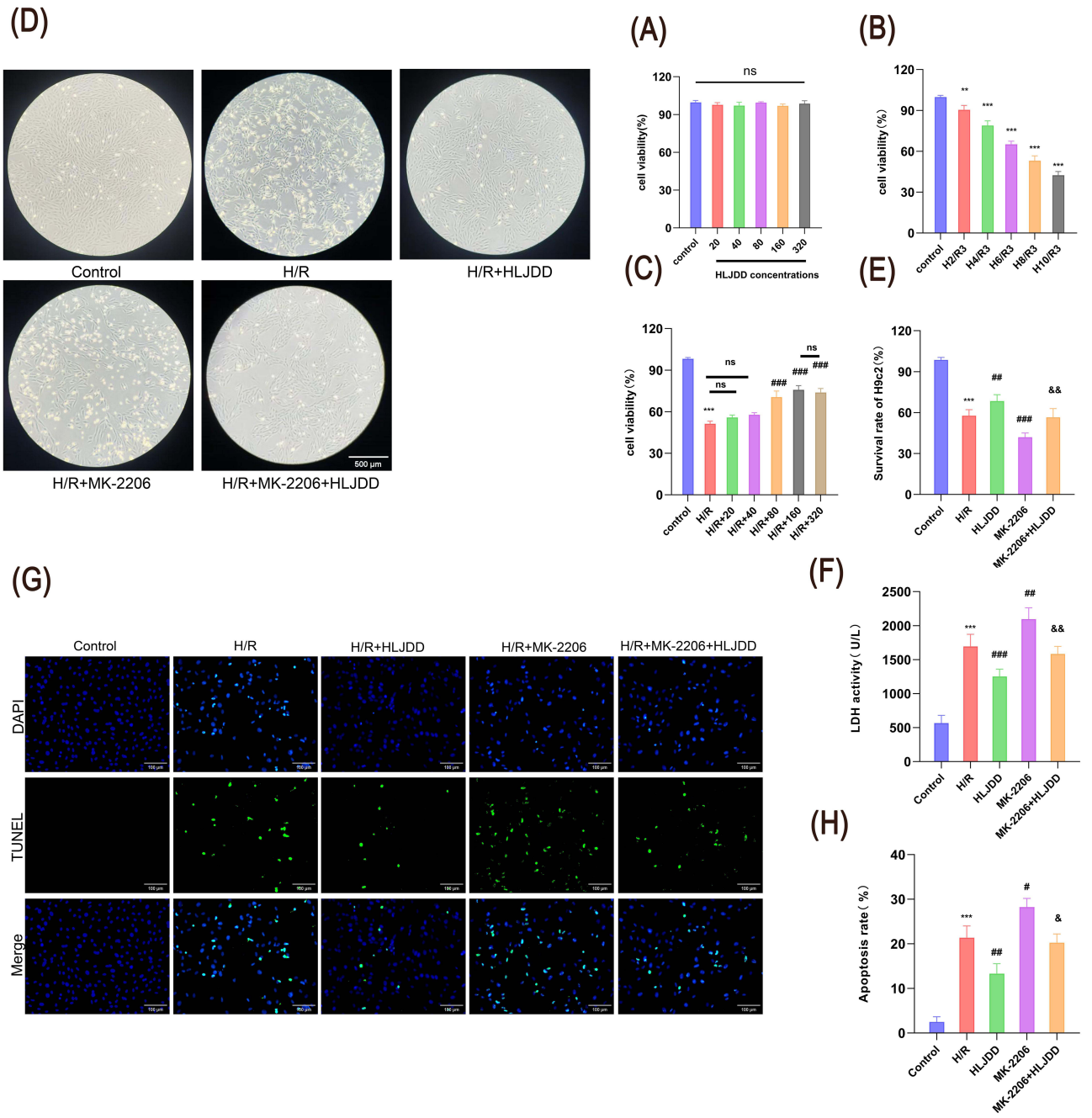

Figure 4 Protective Effects of HLJDD on H9c2 Cells Under H/R Injury. (**A**). HLJDD concentration-dependent effects on cardiomyocyte viability. (**B**). Cell viability after hypoxia 0–10 h and 3 h reoxygenation (n=3). (**C**). Cell viability under H8h/R3h with HLJDD 0–320 μg/mL (n=3). (**D**). Representative microscopic images of H9c2 cells (scale bar: 500μm; n=3). (**E**). Survival rate of H9c2 cells under different treatments (n=5). (**F**). LDH activity in cardiomyocytes (n=5). (**G** and **H**).TUNEL assay images and quantitative analysis (scale bar: 100 μm; TUNEL: green; DAPI: blue; n=3)(Some of the green fluorescence signals in DAPI are due to the entry of fluorescence into the nucleus after apoptosis leads to nuclear pyknosis and changes in membrane permeability).

Notes: Data expressed as mean ± SD. **P<0.01, ***P<0.001 vs Control group; #P<0.05, ##P<0.01, ###P<0.001 vs H/R group; andP<0.05, andandP<0.01 vs HLJDD group; ns: no significance.

followed by 3- hour reoxygenation, yielded a median lethal concentration (Figure 4B). This condition was adopted for subsequent model establishment. For further exploration, after treating cardiomyocytes with different concentrations (0, 20, 40, 80, 160, 320 μg/mL) of HLJDD for 24 hours, the cells were exposed to hypoxia for 8 hours and then reoxygenated for 3 hours to establish a hypoxia/reoxygenation (H/R) model. The cell viability of cardiomyocytes in each group was detected by the Cell Counting Kit-8 (CCK8) method. CCK-8 assays (Figure 4C) demonstrated that HLJDD concentrations of 80–320 μg/mL significantly improved cell viability compared to the H/R model group (all $P < 0.001$), with maximum survival observed at 160 μg/mL. Thus, 160 μg/mL HLJDD was selected for further experiments.

Morphological analysis (Figure 4D) revealed marked differences among experimental groups. Compared to the control group, the H/R model group exhibited reduced cell density, increased floating cells, and adherent cells with shrunken, rounded morphology and compromised membrane integrity. In contrast, HLJDD-treated cells displayed enhanced density, regular morphology in spindle or polygonal shapes, and improved adherence. Especially, AKT inhibition MK-2206 exacerbated H/R-induced damage, further reducing cell density and increasing cellular disintegration, which was partially reversed by HLJDD co-treatment.

From the results of cell viability and LDH activity (Figure 4E and F), it demonstrated that the H/R treatment decreased the cell viability by approximately 0.4 times ($P < 0.001$) and increased the LDH level by about 2 times ($P < 0.001$). HLJDD pretreatment increased viability by 18.5% ($P < 0.01$) and reduced LDH levels by 26% ($P < 0.001$) compared to the H/R group. Conversely, MK-2206 further suppressed viability ($P < 0.001$) and amplified LDH release ($P < 0.01$), abrogating HLJDD-mediated cytoprotection.

AKT Signaling Drives HLJDD's Suppression of H/R-Induced Apoptosis and Ultrastructural Damage

TUNEL staining (Figure 4G and H) showed that the H/R treatment increased apoptotic cells to 21.39 ± 2.65%, whereas HLJDD reduced apoptosis to 13.32 ± 2.25% ($P < 0.01$). MK-2206 treatment elevated apoptosis ($P < 0.05$) and partially negated HLJDD's anti-apoptotic effects ($P < 0.05$).

Transmission electron microscopy (Figure 5A) revealed mitochondrial swelling, cristae deformation, vacuolization, and ER dilation in H/R-injured cells. HLJDD pretreatment restored mitochondrial integrity and alleviated ER swelling. MK-2206 aggravated ultrastructural damage, inducing pronounced ER expansion, autophagosome formation, and mitochondrial vacuolization, which were partially rescued by HLJDD.

HLJDD Alleviates H/R-Induced Endoplasmic Reticulum Stress via AKT Activation

Immunofluorescence (Figure 5B–E) manifested elevated GRP78 (37.42 ± 2.95 vs 8.43 ± 0.72, $P < 0.001$) and CHOP (33.16 ± 3.86 vs 6.82 ± 1.46, $P < 0.001$) expression in the H/R group. HLJDD downregulated GRP78 (25.87 ± 2.31, $P < 0.01$) and CHOP (21.15 ± 1.67, $P < 0.01$). MK-2206 further increased GRP78 ($P < 0.01$) and CHOP ($P < 0.05$), while HLJDD co-treatment attenuated these effects (GRP78: 35.10 ± 2.97 vs 25.87 ± 2.31, $P < 0.01$; CHOP: 32.38 ± 4.03 vs 21.15 ± 1.67, $P < 0.05$).

Moreover, WB (Figure 6A–F) confirmed that H/R upregulated GRP78, p-PERK, p-eIF2α, and CHOP (all $P < 0.001$) while suppressing p-AKT ($P < 0.01$). HLJDD reversed these trends, reducing ERS markers (GRP78: $P < 0.01$; p-PERK: $P < 0.05$; p-eIF2α: $P < 0.01$; CHOP: $P < 0.05$) and enhancing p-AKT ($P < 0.05$). MK-2206 exacerbated ERS ($P < 0.05$) and diminished p-AKT ($P < 0.05$), counteracting HLJDD's benefits. At the same time, qPCR results paralleled these findings (Figure 6G–J).

The above results indicate that pretreatment with HLJDD can alleviate ERS induced by H/R in H9c2 cells, and it is highly likely to act by activating the phosphorylation of AKT and inhibiting the PERK/eIF2α/CHOP pathway.

Discussion

Myocardial ischemia-reperfusion injury (MIRI), a clinically prevalent cardiovascular condition second only to acute myocardial infarction (AMI) in incidence, poses a significant global public health burden.[27] Current studies confirm that oxidative stress, calcium homeostasis imbalance, energy metabolism derangements, inflammatory cascade activation, programmed cell death (including apoptosis, pyroptosis, and ferroptosis) and autophagy dysregulation collectively contribute to MIRI pathogenesis.[28]

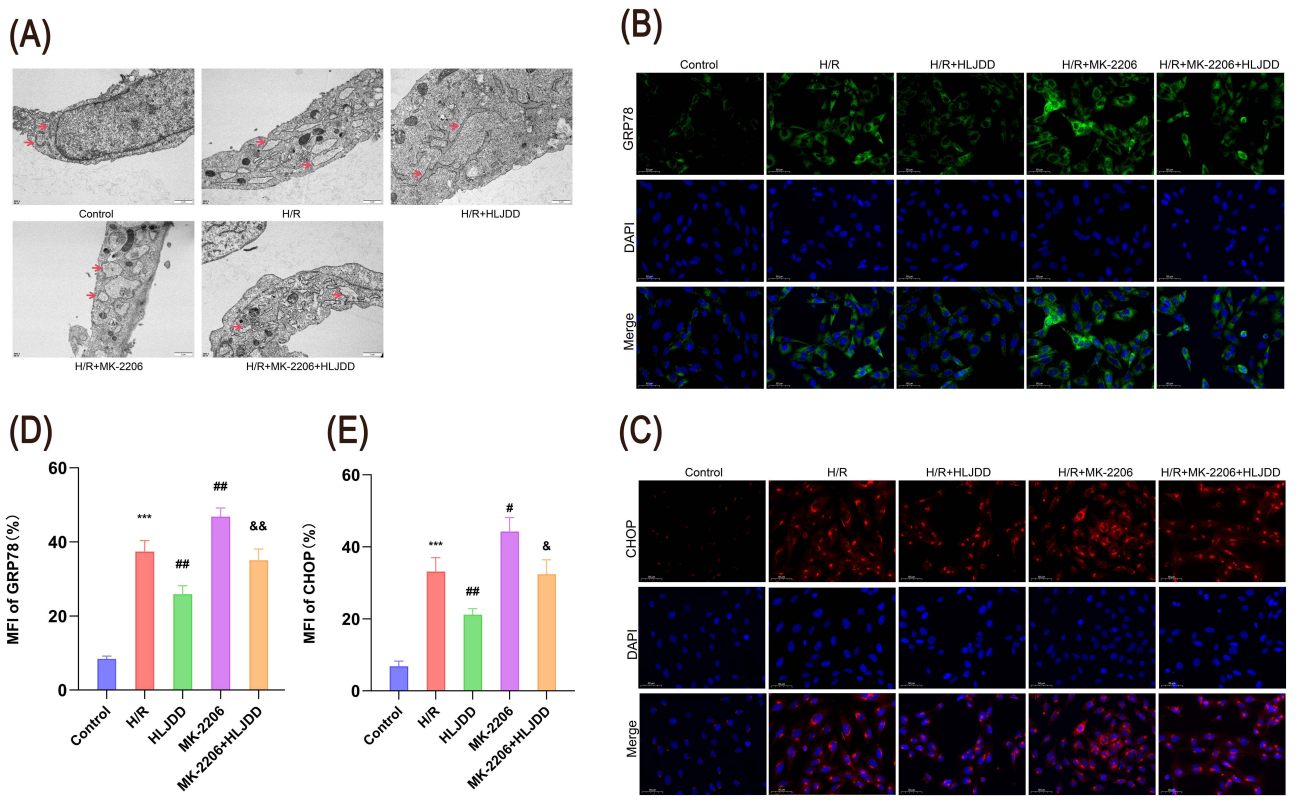

Figure 5 HLJDD Attenuates H/R-Induced ER Expansion and GRP78/CHOP Expression via AKT (**A**). Ultrastructural TEM images of H9c2 cells (red arrows: endoplasmic reticulum; scale bar: 1μm; n=3). (**B** and **D**). GRP78 immunofluorescence images and quantification (scale bar:50μm; GRP78: green; DAPI: blue; n=3). (**C** and **E**). CHOP immunofluorescence images and quantification (scale bar: 50μm; CHOP: red; DAPI: blue; n=3).
Notes: Data expressed as mean ± SD. ***P<0.001 vs Control group; #P<0.05, ##P<0.01 vs H/R group; andP<0.05, andandP<0.01 vs HLJDD group.

Traditional Chinese Medicine (TCM) interventions for MIRI have gained prominence in cardiovascular research. Large-scale multicenter clinical trials demonstrate TCM's unique advantages in regulating complex pathological networks and therapeutically relevant modulation of such networks.[29] Pharmacological evaluations confirm the safety of TCM formulations within clinical dosage ranges, with no significant adverse events reported in experimental or clinical studies.[29,30] Large-scale, multicenter clinical trials have demonstrated that traditional Chinese medicine (TCM) formulae exert therapeutically relevant modulation of complex pathological networks. Rationally combining these botanical preparations with standard-of-care pharmacotherapies further reduces toxicity while enhancing efficacy.[31] Huanglian Jiedu Decoction (HLJDD) exhibits therapeutic efficacy in atherosclerosis, hypertension, sepsis, and type 2 diabetes by neuraminidase inhibition, hypoxic microenvironment improvement, and apoptosis regulation.[32–34] Animal studies reveal that oral HLJDD (2.5−5.0 g/kg/d) ameliorates cardiac remodeling in transverse aortic constriction models, as evidenced by improved cardiac function, reduced interstitial fibrosis, and decreased inflammatory infiltration.[35] Nevertheless, its precise mechanism in MIRI remain unclear.

This study systematically investigates HLJDD's regulatory effects on ERS-mediated apoptosis during MIRI, particularly focusing on molecular crosstalk between H/R-induced ERS and AKT signaling. We established an in vivo MIRI model via 30 minutes of ischemia followed by 2 hours of reperfusion, using the clinically applied anti-ERS drug nicorandil as a positive control,[36,37] results demonstrate significantly elevated serum lactate dehydrogenase (LDH) and creatine kinase-MB (CK-MB) levels in the model group compared with the sham control group, accompanied by severe pathological damage, an increased apoptotic index (Bax/Bcl-2 ratio), and upregulated cleaved-caspase 3 expression. Both HLJDD dose groups and the nicorandil group showed varying degrees of improvement, with high-dose HLJDD exhibiting efficacy comparable to that of nicorandil. These findings indicate that HLJDD protects rats against MIRI to some extent.

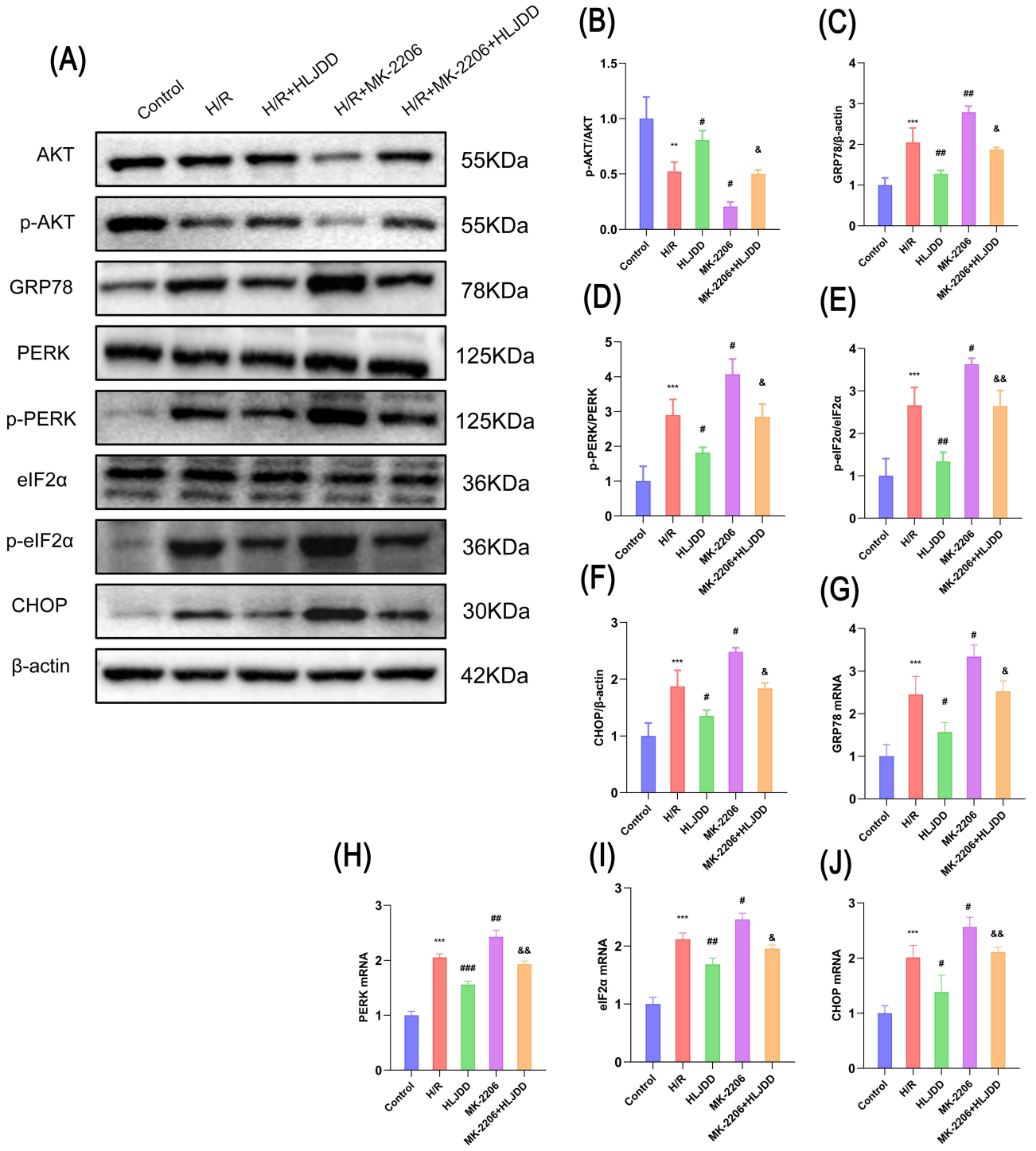

Figure 6 HLJDD Reduces H/R-Induced ER Stress Proteins and mRNA via AKT. (**A**–**F**). Western blotting and quantification of p-AKT, AKT, GRP78, p-PERK, PERK, p-eIF2α, eIF2α, and CHOP (n=3). (**G**–**J**). mRNA levels of GRP78, PERK, eIF2α, and CHOP (n=3).
Notes: Data expressed as mean ± SD. **P<0.01, ***P<0.001 vs Control group; #P<0.05, ##P<0.01, ###P<0.001 vs H/R group; andP<0.05, andandP<0.01 vs HLJDD group.

Next, we systematically investigated the therapeutic targets and molecular mechanisms of HLJDD in improving MIRI via network pharmacology. These 8 core targets are mainly involved in regulating apoptosis and ERS-related pathways. AKT1, a key member of the protein kinase B (PKB) family, modulates cell survival via phosphorylation-dependent mechanisms.[38,39] Experimental evidence confirms that activating the PI3K/AKT pathway counteracts apoptosis and regulates myocardial

https://doi.org/10.2147/JIR.S535348

contractility during ischemia-reperfusion.[40–42] MAPK1, a mitogen-activated protein kinase, integrates oxidative stress signaling and contributes to cardiovascular pathologies.[43,44]

Gene Ontology (GO) analysis showed that HLJDD's cardioprotective targets are mainly involved in regulating apoptosis, responding to exogenous stimuli, and adapting to hypoxia. These targets are significantly enriched in membrane microdomains and the endoplasmic reticulum (ER) lumen, with protein binding as the principal molecular function. The ER is the main organelle that controls protein synthesis, folding, post-translational modification, and Ca^2+ homeostasis, and is highly sensitive to metabolic stress.[45,46] During ischemia/hypoxia, accumulating unfolded or misfolded proteins in the lumen initiates ERS and subsequently activates the unfolded protein response (UPR)—an evolutionarily conserved cytoprotective program.[47] However, prolonged or excessive UPR signaling shifts from adaptive to pro-apoptotic, and aberrant ERS contributes to various cardiovascular pathologies, including MIRI and atherosclerosis.[48–50] Sustained ERS promotes programmed cell death by upregulating C/EBP homologous protein (CHOP), activating caspase-12, and via c-Jun N-terminal kinase (JNK)-mediated signaling.[51–53] Thus, persistent ERS and its downstream apoptotic cascades are critical drivers of MIRI pathogenesis.[54,55]

KEGG pathway analysis further confirmed that HLJDD may affect the pathological progression of MIRI by modulating the PI3K/AKT signaling axis and ERS-related pathways, including Pathways in cancer and Lipid and atherosclerosis. (See the mechanism diagram in Supplementary Figures 1–4).

Despite its utility, network pharmacology is inherently limited by inconsistent topological algorithms and the lack of standardized quality metrics for input data. Its reliance on literature-curated interactomes overweights well-characterized pathways and proteins, thus systematically introducing confirmation bias and spurious "irrelevant" targets into predicted therapeutic networks. Therefore, we did not confine our investigation to top-ranked mechanisms/pathways. By reviewing relevant literature, integrating our research group's previous experimental data[15,19] and considering our preliminary findings (significantly upregulated GRP78 expression in the model group and marked downregulation after HLJDD intervention), we specifically focused on ERS mechanisms to elucidate their regulatory role in HLJDD-mediated MIRI alleviation.

In this study, we established an in vitro ischemia/reperfusion (I/R) injury model via 8 hours of hypoxia followed by 3 hours of reoxygenation (H/R). Results showed that H/R stimulation induced severe cell damage, as evidenced by increased LDH activity, elevated apoptosis rate, decreased cell viability, and morphological changes. HLJDD intervention significantly attenuated these pathological changes, confirming its cardioprotective effects against H/R-induced injury.

The initiation of ERS is marked by GRP78 upregulation.[56] Upon GRP78 dissociation, three signaling branches—PERK, IRE1α, and ATF6—are activated. Immunofluorescence staining, Western blotting, and qPCR results showed that H/R injury induced GRP78 upregulation compared with the control group, indicating that H/R injury triggered excessive ERS. Additionally, increased CHOP expression confirmed that H/R injury activated the ERS-mediated CHOP apoptotic pathway. Transmission electron microscopy further confirmed that H/R-treated cells had ultrastructural damage, including mitochondrial cristae swelling and rupture, and endoplasmic reticulum dilation. These results are consistent with those reported by Yue et al[57] and Gan et al[57,58] ERS induces GRP78 dissociation from PERK. Activated PERK then increases eIF2α phosphorylation and promotes CHOP transcriptional activation, which triggers cell death and thus induces apoptosis. Our results indicate that HLJDD pretreatment protects against I/R-induced myocardial injury by attenuating ERS-related apoptosis.

Mechanistically, we identified AKT signaling as a critical regulator of PERK-mediated ERS. H/R injury significantly decreased the p-AKT/AKT ratio, which was effectively reversed by HLJDD pretreatment. Intriguingly, co-administration of the AKT-specific inhibitor MK-2206 abolished HLJDD-mediated cardioprotection, as evidenced by the reappearance of ERS markers and exacerbation of cell impairment, indicating that AKT activation is essential for HLJDD's therapeutic effects. Previous studies have shown that naringenin significantly enhances the viability of H/R-treated H9c2 cells and inhibits cell apoptosis.[59] It also reduces ERS-related protein levels and suppresses the activation of pathways such as ATF6, IRE1α, and PERK. Basic fibroblast growth factor (bFGF) has been demonstrated to ameliorate ERS and mitochondrial dysfunction in animal models by activating the PI3K/AKT pathway.[60] Berberine—the core active component of *Coptis chinensis* Franch and a major bioactive constituent of HLJDD—exerts similar cardioprotective effects by regulating ERS.[61] Our study's data extend these findings, confirming that HLJDD regulates the AKT/PERK axis.

The innovation of this study lies in its focus on a novel mechanism: HLJDD effectively alleviates ERS-dependent apoptosis by activating the AKT signaling pathway to inhibit the PERK/eIF2α pathway, thereby ultimately ameliorating

H/R-induced cardiomyocyte injury. From a translational medicine perspective, this study not only provides a theoretical basis for developing novel ERS inhibitors but, more importantly, identifies the molecular targets of this traditional Chinese medicine (TCM) compound prescription using modern molecular biology techniques—paving a new path for its modern application in the prevention and treatment of cardiovascular diseases.

Limitations and Future Directions

Despite its meaningful findings, this study has several limitations.

First, mechanistic validation is incomplete. While HLJDD's efficacy in myocardial ischemia/reperfusion (I/R)-like injury was confirmed via animal histopathology and apoptotic markers, the "in vivo ERS-related pathway mechanism lacks direct verification". For the AKT pathway, only phosphorylated AKT (p-AKT) was analyzed (no PI3K, mTOR, or GSK-3β), weakening mechanistic support. Additionally, relying solely on an AKT inhibitor (no genetic knockout) introduces uncertainty due to potential off-target effects.

Second, models limit clinical extrapolation. In vitro studies used only H9c2 cells (rat cardiomyoblasts), which differ from primary human cardiomyocytes in function and metabolism. No validation in human-derived models (eg, hiPSC-derived cardiomyocytes) further hinders translation.

Third, key pharmacologic and clinical data are missing: no HLJDD pharmacokinetic or mass spectrometry (active component) analyses, nor clinical relevance insights (eg, patient correlations), limiting practical value.

Fourth, ERS crosstalk with inflammation, autophagy, or oxidative stress (critical in myocardial I/R) was unexamined, precluding a holistic mechanism understanding.

Future work should: (1) Validate in vivo ERS/AKT pathways; (2) Test in human-derived models with clinical analyses; (3) Conduct HLJDD pharmacologic/component studies; (4) Explore ERS crosstalk; (5) Combine pharmacologic inhibition with genetic manipulation (eg, AKT knockout). These steps will boost reliability and translational potential.

Abbreviations

HLJDD, Huanglian Jiedu Decoction; AKT, RAC-Alpha Serine/Threonine-Protein Kinase; BP, biological process; CC, cell composition; MF, molecular function; DAVID, Database for Annotation, Visualization and Integrated; GO, Gene Ontology; KEGG, Kyoto Encyclopedia of Genes and Genomes; PPI, protein-protein interaction; ERS, Endoplasmic Reticulum stress; ER, endoplasmic reticulum; MIRI, Myocardial ischemia reperfusion injury; H/R, hypoxia/re-oxygenation; GRP78, Glucose-regulated protein 78; PERK, Protein kinase R-like endoplasmic reticulum kinase; EIF2A, Eukaryotic translation initiation factor 2α; CHOP, C/EBP-homologous protein; DAPI, 4',6-diamidino-2-phenylindole; DMEM, Dulbecco's Modified Eagle Medium; LDH, lactate dehydrogenase; CK-MB, Creatine Kinase Mb; Qpcr, Quantitative Real-time polymerase chain reaction; WB, Western blotting; UPR, unfolded protein response.

Data Sharing Statement

The data generated in this study are available from the last corresponding author (Yijun Qiu) on reasonable request.

Acknowledgments

Lingnan Medical Research Center of Guangzhou University of Chinese Medicine and Science and Technology Innovation Center of Guangzhou University of Chinese Medicine must be given great thanks for providing the technologies. Also, I would like to express my sincere gratitude to BioRender for its invaluable assistance in the process of figure creation. Graphical abstract Created in BioRender. gu, m. (2025) https://BioRender.com/zoyzott.

Author Contributions

All authors made a significant contribution to the work reported, whether that is in the conception, study design, execution, acquisition of data, analysis and interpretation, or in all these areas; took part in drafting, revising or critically reviewing the article; gave final approval of the version to be published; have agreed on the journal to which the article has been submitted; and agree to be accountable for all aspects of the work.

Funding

This work was supported by the Guangzhou Science and Technology Plan Project (Grant No. 202201020358 to Y. J. Q.), the Scientific Research Project of Guangdong Provincial Administration of Traditional Chinese Medicine (Grant No. 20251105 to R. L.), and the Natural Science Foundation of Guangdong Province (Grant No. 2021A1515011465).

Disclosure

The authors declare that the research was conducted in the absence of any commercial or financial relationships that could be construed as a potential conflict of interest.

References

1. Giricz Z, Varga ZV, Baranyai T, et al. Cardioprotection by remote ischemic preconditioning of the rat heart is mediated by extracellular vesicles. *J Mol Cell Cardiol*. 2014;68:75–78. doi:10.1016/j.yjmcc.2014.01.004
2. Sun J, Nguyen T, Aponte AM, et al. Ischaemic preconditioning preferentially increases protein S-nitrosylation in subsarcolemmal mitochondria. *Cardiovasc Res*. 2015;106(2):227–236. doi:10.1093/cvr/cvv044
3. Nakano S, Kohsaka S, Chikamori T, et al. JCS 2022 guideline focused update on diagnosis and treatment in patients with stable coronary artery disease. *Circ J*. 2022;86(5):882–915. doi:10.1253/circj.CJ-21-1041
4. Perricone AJ, Vander Heide RS. Novel therapeutic strategies for ischemic heart disease. *Pharmacol Res*. 2014;89:36–45. doi:10.1016/j.phrs.2014.08.004
5. Scarabelli TM, Gottlieb RA. Functional and clinical repercussions of myocyte apoptosis in the multifaceted damage by ischemia/reperfusion injury: old and new concepts after 10 years of contributions. *Cell Death Differ*. 2004;11 Suppl 2:S144–152. doi:10.1038/sj.cdd.4401544
6. Li H, Zhu X, Fang F, Jiang D, Tang L. Down-regulation of GRP78 enhances apoptosis via CHOP pathway in retinal ischemia-reperfusion injury. *Neurosci Lett*. 2014;575:68–73. doi:10.1016/j.neulet.2014.05.042
7. Urra H, Dufey E, Lisbona F, Rojas-Rivera D, Hetz C. When ER stress reaches a dead end. *Biochim Biophys Acta*. 2013;1833(12):3507–3517. doi:10.1016/j.bbamcr.2013.07.024
8. Wang T, Li X, Yang D, et al. ER stress and ER stress-mediated apoptosis are involved in manganese-induced neurotoxicity in the rat striatum in vivo. *Neurotoxicology*. 2015;48:109–119. doi:10.1016/j.neuro.2015.02.007
9. Wolfrum S, Dendorfer A, Rikitake Y, et al. Inhibition of Rho-kinase leads to rapid activation of phosphatidylinositol 3-kinase/protein kinase Akt and cardiovascular protection. *Arterioscler Thromb Vasc Biol*. 2004;24(10):1842–1847. doi:10.1161/01.ATV.0000142813.33538.82
10. Hu P, Han Z, Couvillon AD, Exton JH. Critical role of endogenous Akt/IAPs and MEK1/ERK pathways in counteracting endoplasmic reticulum stress-induced cell death. *J Biol Chem*. 2004;279(47):49420–49429. doi:10.1074/jbc.M407700200
11. Hyoda K, Hosoi T, Horie N, Okuma Y, Ozawa K, Nomura Y. PI3K-Akt inactivation induced CHOP expression in endoplasmic reticulum-stressed cells. *Biochem Biophys Res Commun*. 2006;340(1):286–290. doi:10.1016/j.bbrc.2005.12.007
12. K HAT, Mahfoudh Boussaid A, Zaouali MA, et al. Melatonin modulates endoplasmic reticulum stress and Akt/GSK3-beta signaling pathway in a rat model of renal warm ischemia reperfusion. *Anal Cell Pathol*. 2015;2015:635172. doi:10.1155/2015/635172
13. Yang Y, Wang HJ, Yang J, et al. Chemical profiling and quantification of Chinese medicinal formula Huang-Lian-Jie-Du decoction, a systematic quality control strategy using ultra high performance liquid chromatography combined with hybrid quadrupole-orbitrap and triple quadrupole mass spectrometers. *J Chromatogr A*. 2013;1321:88–99. doi:10.1016/j.chroma.2013.10.072
14. Liu H, Chen X, Liu Y, Fang C, Chen S. Antithrombotic effects of Huanglian Jiedu decoction in a rat model of ischaemia-reperfusion-induced cerebral stroke. *Pharm Biol*. 2021;59(1):823–827. doi:10.1080/13880209.2021.1942505
15. Lin J, Gu M, Wang X, et al. Huanglian Jiedu decoction inhibits vascular smooth muscle cell-derived foam cell formation by activating autophagy via suppressing P2RY12. *J Ethnopharmacol*. 2024;328:118125. doi:10.1016/j.jep.2024.118125
16. Chan E, Liu XX, Guo DJ, et al. Extract of Scutellaria baicalensis Georgi root exerts protection against myocardial ischemia-reperfusion injury in rats. *Am J Chin Med*. 2011;39(4):693–704. doi:10.1142/S0192415X11009135
17. Huang Z, Han Z, Ye B, et al. Berberine alleviates cardiac ischemia/reperfusion injury by inhibiting excessive autophagy in cardiomyocytes. *Eur J Pharmacol*. 2015;762:1–10. doi:10.1016/j.ejphar.2015.05.028
18. Kim YM, Ha YM, Jin YC, et al. Palmatine from Coptidis rhizoma reduces ischemia-reperfusion-mediated acute myocardial injury in the rat. *Food Chem Toxicol*. 2009;47(8):2097–2102. doi:10.1016/j.fct.2009.05.031
19. Li R, Zhang J, Ji S, et al. Qingre Huoxue decoction attenuates myocardial ischemia–reperfusion injury by regulating the autophagy–endoplasmic reticulum stress axis via FAM134B-mediated ER-phagy. *Front Pharmacol*. 2024;15:1447610. doi:10.3389/fphar.2024.1447610
20. Ye J, Lyu TJ, Li LY, et al. Ginsenoside Re attenuates myocardial ischemia/reperfusion induced ferroptosis via miR-144-3p/SLC7A11. *Phytomedicine*. 2023;113:154681. doi:10.1016/j.phymed.2023.154681
21. Yao D, Bao L, Wang S, et al. Isoliquiritigenin alleviates myocardial ischemia-reperfusion injury by regulating the Nrf2/HO-1/SLC7a11/GPX4 axis in mice. *Free Radic Biol Med*. 2024;221:1–12. doi:10.1016/j.freeradbiomed.2024.05.012
22. Li M, Meng Z, Yu S, et al. Baicalein ameliorates cerebral ischemia-reperfusion injury by inhibiting ferroptosis via regulating GPX4/ACSL4/ACSL3 axis. *Chem Biol Interact*. 2022;366:110137. doi:10.1016/j.cbi.2022.110137
23. Hamosh A, Scott AF, Amberger J, Valle D, McKusick VA. Online Mendelian Inheritance in Man (OMIM). *Hum Mutat*. 2000;15(1):57–61. doi:10.1002/(SICI)1098-1004(200001)15:1<57::AID-HUMU12>3.0.CO;2-G
24. Pinero J, Ramirez-Anguita JM, Sauch-Pitarch J, et al. The DisGeNET knowledge platform for disease genomics: 2019 update. *Nucleic Acids Res*. 2020;48(D1):D845–D855. doi:10.1093/nar/gkz1021
25. Stelzer G, Rosen N, Plaschkes I, et al. The GeneCards Suite: from gene data mining to disease genome sequence analyses. *Curr Protoc Bioinformatics*. 2016;54(1):3031–313033. doi:10.1002/cpbi.5

26. Xiang H, Yang J, Li J, et al. Citrate pretreatment attenuates hypoxia/reoxygenation-induced cardiomyocyte injury via regulating microRNA-142-3p/Rac1 aix. *J Recept Signal Transduction Res*. 2020;40(6):560–569. doi:10.1080/10799893.2020.1768548
27. Ibanez B, Heusch G, Ovize M, Van de Werf F. Evolving therapies for myocardial ischemia/reperfusion injury. *J Am Coll Cardiol*. 2015;65(14):1454–1471. doi:10.1016/j.jacc.2015.02.032
28. Zhang S, Yan F, Luan F, et al. The pathological mechanisms and potential therapeutic drugs for myocardial ischemia reperfusion injury. *Phytomedicine*. 2024;129:155649. doi:10.1016/j.phymed.2024.155649
29. Yang Y, Li X, Chen G, et al. Traditional Chinese Medicine Compound (Tongxinluo) and clinical outcomes of patients with acute myocardial infarction: the CTS-AMI randomized clinical trial. *JAMA*. 2023;330(16):1534–1545. doi:10.1001/jama.2023.19524
30. Zhang S, Bai X, Chen ZL, Li JJ, Chen YY, Tang YP. Qiju Dihuang Decoction for hypertension: a systematic review and meta-analysis. *Evid Based Complement Alternat Med*. 2020;2020:9403092. doi:10.1155/2020/9403092
31. Zhang Q, Shi J, Guo D, et al. Qishen Granule alleviates endoplasmic reticulum stress-induced myocardial apoptosis through IRE-1-CRYAB pathway in myocardial ischemia. *J Ethnopharmacol*. 2020;252:112573. doi:10.1016/j.jep.2020.112573
32. Zhang JY, Chen QQ, Li J, Zhang L, Qi LW. Neuraminidase 1 and its inhibitors from Chinese Herbal medicines: an emerging role for cardiovascular diseases. *Am J Chin Med*. 2021;49(4):843–862. doi:10.1142/S0192415X21500403
33. Li X, Wei S, Niu S, et al. Network pharmacology prediction and molecular docking-based strategy to explore the potential mechanism of Huanglian Jiedu Decoction against sepsis. *Comput Biol Med*. 2022;144:105389. doi:10.1016/j.compbiomed.2022.105389
34. Yin B, Bi YM, Fan GJ, Xia YQ. Molecular mechanism of the effect of Huanglian Jiedu Decoction on type 2 diabetes mellitus based on network pharmacology and molecular docking. *J Diabetes Res*. 2020;2020:5273914. doi:10.1155/2020/5273914
35. Chen QQ, Wang FX, Cai YY, et al. Untargeted metabolomics and lipidomics uncovering the cardioprotective effects of Huanglian Jiedu Decoction on pathological cardiac hypertrophy and remodeling. *J Ethnopharmacol*. 2021;270:113646. doi:10.1016/j.jep.2020.113646
36. Liu Z, Han X, You Y, et al. Shuangshen ningxin formula attenuates cardiac microvascular ischemia/reperfusion injury through improving mitochondrial function. *J Ethnopharmacol*. 2024;323:117690. doi:10.1016/j.jep.2023.117690
37. Zheng Y, Li X, Zhang F, et al. Protective effect of nicorandil against myocardial ischemia/reperfusion injury mediated via IL33/ST2 signaling pathway. *Mol Cell Biochem*. 2022;477(7):1921–1929. doi:10.1007/s11010-022-04418-z
38. Song X, Wang Z, Liang H, et al. Dioscin induces gallbladder cancer apoptosis by inhibiting ROS-mediated PI3K/AKT signalling. *Int J Biol Sci*. 2017;13(6):782–793. doi:10.7150/ijbs.18732
39. Tao SC, Yuan T, Rui BY, Zhu ZZ, Guo SC, Zhang CQ. Exosomes derived from human platelet-rich plasma prevent apoptosis induced by glucocorticoid-associated endoplasmic reticulum stress in rat osteonecrosis of the femoral head via the Akt/Bad/Bcl-2 signal pathway. *Theranostics*. 2017;7(3):733–750. doi:10.7150/thno.17450
40. Li X, Bilali A, Qiao R, Paerhati T, Yang Y. Association of the PPARgamma/PI3K/Akt pathway with the cardioprotective effects of tacrolimus in myocardial ischemic/reperfusion injury. *Mol Med Rep*. 2018;17(5):6759–6767. doi:10.3892/mmr.2018.8649
41. Tabe Y, Jin L, Konopleva M, et al. Class IA PI3K inhibition inhibits cell growth and proliferation in mantle cell lymphoma. *Acta Haematol*. 2014;131(1):59–69. doi:10.1159/000353164
42. Zhou HM, Sun QX, Cheng Y. Paeonol enhances the sensitivity of human ovarian cancer cells to radiotherapy-induced apoptosis due to downregulation of the phosphatidylinositol-3-kinase/Akt/phosphatase and tensin homolog pathway and inhibition of vascular endothelial growth factor. *Exp Ther Med*. 2017;14(4):3213–3220. doi:10.3892/etm.2017.4877
43. Wu M, Xing Q, Duan H, Qin G, Sang N. Suppression of NADPH oxidase 4 inhibits PM(2.5)-induced cardiac fibrosis through ROS-P38 MAPK pathway. *Sci Total Environ*. 2022;837:155558. doi:10.1016/j.scitotenv.2022.155558
44. Lv S, Ju C, Peng J, et al. 25-Hydroxycholesterol protects against myocardial ischemia-reperfusion injury via inhibiting PARP activity. *Int J Biol Sci*. 2020;16(2):298–308. doi:10.7150/ijbs.35075
45. Roussel BD, Kruppa AJ, Miranda E, Crowther DC, Lomas DA, Marciniak SJ. Endoplasmic reticulum dysfunction in neurological disease. *Lancet Neurol*. 2013;12(1):105–118. doi:10.1016/S1474-4422(12)70238-7
46. Groenendyk J, Agellon LB, Michalak M. Calcium signaling and endoplasmic reticulum stress. *Int Rev Cell Mol Biol*. 2021;363:1–20.
47. Di Conza G, Ho PC. ER stress responses: an emerging modulator for innate immunity. *Cells*. 2020;9(3). doi:10.3390/cells9030695
48. Xu C, Bailly-Maitre B, Reed JC. Endoplasmic reticulum stress: cell life and death decisions. *J Clin Invest*. 2005;115(10):2656–2664. doi:10.1172/JCI26373
49. Groenendyk J, Agellon LB, Michalak M. Coping with endoplasmic reticulum stress in the cardiovascular system. *Annu Rev Physiol*. 2013;75:49–67. doi:10.1146/annurev-physiol-030212-183707
50. Tao J, Zhu W, Li Y, et al. Apelin-13 protects the heart against ischemia-reperfusion injury through inhibition of ER-dependent apoptotic pathways in a time-dependent fashion. *Am J Physiol Heart Circ Physiol*. 2011;301(4):H1471–1486. doi:10.1152/ajpheart.00097.2011
51. Fu HY, Sanada S, Matsuzaki T, et al. Chemical endoplasmic reticulum chaperone alleviates doxorubicin-induced cardiac dysfunction. *Circ Res*. 2016;118(5):798–809. doi:10.1161/CIRCRESAHA.115.307604
52. Li X, Zhang X, Yan B. Ab initio study on the low-lying excited states of gas-phase PH(+) cation including spin-orbit coupling. *Spectrochim Acta A Mol Biomol Spectrosc*. 2015;142:1–7. doi:10.1016/j.saa.2015.01.070
53. Boyce M, Yuan J. Cellular response to endoplasmic reticulum stress: a matter of life or death. *Cell Death Differ*. 2006;13(3):363–373. doi:10.1038/sj.cdd.4401817
54. Teng X, Song J, Zhang G, et al. Inhibition of endoplasmic reticulum stress by intermedin(1-53) protects against myocardial injury through a PI3 kinase-Akt signaling pathway. *J Mol Med*. 2011;89(12):1195–1205. doi:10.1007/s00109-011-0808-5
55. Xu J, Hu H, Chen B, et al. Lycopene protects against hypoxia/reoxygenation injury by alleviating ER stress induced apoptosis in neonatal mouse cardiomyocytes. *PLoS One*. 2015;10(8):e0136443. doi:10.1371/journal.pone.0136443
56. Gupta MK, Tahrir FG, Knezevic T, et al. GRP78 interacting partner Bag5 responds to ER stress and protects cardiomyocytes from ER stress-induced apoptosis. *J Cell Biochem*. 2016;117(8):1813–1821. doi:10.1002/jcb.25481
57. Gan R, Hu G, Zhao Y, et al. Post-conditioning protecting rat cardiomyocytes from apoptosis via attenuating calcium-sensing receptor-induced endo(sarco)plasmic reticulum stress. *Mol Cell Biochem*. 2012;361(1–2):123–134. doi:10.1007/s11010-011-1096-7
58. Yue R, Lv M, Lan M, et al. Irisin protects cardiomyocytes against hypoxia/reoxygenation injury via attenuating AMPK mediated endoplasmic reticulum stress. *Sci Rep*. 2022;12(1):7415. doi:10.1038/s41598-022-11343-0

59. Tang JY, Jin P, He Q, et al. Naringenin ameliorates hypoxia/reoxygenation-induced endoplasmic reticulum stress-mediated apoptosis in H9c2 myocardial cells: involvement in ATF6, IRE1alpha and PERK signaling activation. *Mol Cell Biochem*. 2017;424(1–2):111–122. doi:10.1007/s11010-016-2848-1
60. Wang Z, Wang Y, Ye J, et al. bFGF attenuates endoplasmic reticulum stress and mitochondrial injury on myocardial ischaemia/reperfusion via activation of PI3K/Akt/ERK1/2 pathway. *J Cell Mol Med*. 2015;19(3):595–607. doi:10.1111/jcmm.12346
61. Zhao GL, Yu LM, Gao WL, et al. Berberine protects rat heart from ischemia/reperfusion injury via activating JAK2/STAT3 signaling and attenuating endoplasmic reticulum stress. *Acta Pharmacol Sin*. 2016;37(3):354–367. doi:10.1038/aps.2015.136